Chemical Tuning of Nonlinearity Leading to Intrinsically Localized Modes in Halide-Bridged Mixed-Valence Platinum Materials†

Wayne E. Buschmann,‡,§ Shawn D. McGrane,⊥ and Andrew P. Shreve*,‡

Bioscience Division and Dynamic Experimentation Division, Los Alamos National Laboratory, Los Alamos, New Mexico 87545

Received: January 7, 2003; In Final Form: April 16, 2003

The appearance of nonlinearity in multiphonon excitations is compared in the series of $[Pt(en)_2X_2][Pt(en)_2](ClO_4)_4$ (X = Cl, Br, I; en = ethylenediamine) mixed-valence, linear-chain, charge-density-wave compounds. This comparison is made for crystals obtained under new synthetic conditions that minimize chemical defects incorporated during crystal growth. The single-crystal resonance Raman spectra collected at 77 K on this series (with natural isotope abundances) show strong red-shifting of the X−Pt−X symmetric stretch overtone peaks for X = Cl, modest red-shifting for X = Br, and no anharmonicity for X = I. When X = Cl, by the sixth overtone of the ^{35}Cl−Pt−^{35}Cl stretch, red shifts significantly larger than 10% of the fundamental frequency are observed. In addition, evolution of spectral line shapes corresponding to formation of dynamically localized vibrational states (intrinsically localized modes) is apparent, even by the second overtone. When X = Br, observed red shifts are less than 7% up to the eighth overtone, and there is no spectral evidence for intrinsically localized modes at 77 K. Further study of X = Br at 4 K yields spectra up to the 11th overtone having similar red shifts and narrower line shapes than at 77 K but provides only very ambiguous indications of resolved combination bands that could correspond to intrinsically localized modes. When X = I, the lack of any observed anharmonicity indicates linear phonon excitations, which likely correspond to highly delocalized small amplitude motions. The series of data presented here demonstrate how nonlinearities in vibrational degrees of freedom, and the corresponding existence of localized modes, can be tuned chemically by adjusting the competing effects of electron delocalization and electron−phonon interactions in low-dimensional materials.

I. Introduction

The intrinsic localization of energy in extended systems is an important topic of study in nonlinear science. In particular, the localization of energy in translationally invariant discrete lattices, leading to the formation of so-called intrinsically localized modes (ILMs), is an active area of research.[1−5] ILMs involving vibrational energy can play a role in governing the response of any property that is coupled to vibrational degrees of freedom in such materials and, as such, may influence magnetic, optical, electronic, chemical, and physical properties. Despite their importance and the large number of theoretical studies of ILMs, their experimental observation has been challenging. However, recent studies have demonstrated the formation of localized vibrational states in lattices where nonlinearity is produced by the interplay of electron delocalization interactions and electron−phonon coupling,[3] of localized spin waves in magnetically driven materials,[4] and of localized vibrational states in crystals of acetanilide.[5] The latter case also builds upon earlier work that interpreted infrared absorption line shapes in acetanilide in terms of localized mode (self-trapped vibrational exciton) formation.[6] In addition, local excitations in finite, but degenerate (symmetric), systems have been a topic of much interest. Examples include the study of so-called local mode excitations in molecules, which has been extensively reviewed.[7] More recently, studies of dynamics within arrays of coupled Josephson junctions have provided a means for addressing how nonlinearity can lead to symmetry breaking and localization of energy.[8]

Our group and co-workers have studied, experimentally and theoretically, the appearance of ILMs in a member of the class of materials known as halide-bridged mixed-valence transition-metal compounds.[3,9,10] This general class of materials has been studied for many years.[11−13] The basic structure consists of a linear chain of transition-metal ions with intervening halide ions. The halide ions occupy axial ligand positions of the transition-metal ions, and the equatorial coordination sites are typically occupied by amine-based ligands. The optical and electronic properties of the crystalline materials are highly anisotropic, and the low-energy electronic excitations are along the chain axis. The prototypical example of these materials is $\{[Pt(en)_2Cl_2][Pt(en)_2](ClO_4)_4\}$, often referred to as PtCl (here, en = ethylenediamine).

The structure of PtCl is presented in recent publications.[3,13,14] A hypothetical symmetric ground state would consist of Pt^{3+} sites with an equidistantly spaced Cl^- ion between each pair of Pt ions. The actual structure of the material is obtained by a commensurate Peierls distortion and charge-density wave (CDW) formation away from this hypothetical symmetric state, leading to a ground state in which alternating oxidized ($Pt^{+(3+\delta)}$) and reduced ($Pt^{+(3-\delta)}$) metal sites are found and in which the halide sublattice is distorted toward the oxidized Pt site. The

* Corresponding author: Bioscience Division; MS G755; Los Alamos National Laboratory. E-mail: shreve@lanl.gov. Phone: 505-667-6933. Fax: 505-665-9224.

† Part of the special issue "A. C. Albrecht Memorial Issue".

‡ Bioscience Division, Los Alamos National Laboratory.

§ Current Address: Eltron Research, Inc.; 4600 Nautilus Court South; Boulder, CO 80301.

⊥ Dynamic Experimentation Division, Los Alamos National Laboratory.

10.1021/jp034038k CCC: $25.00
Published on Web 06/07/2003

coupled CDW and Peierls distortion lead to an optical gap that corresponds to an intervalence charge-transfer (IVCT) transition between reduced and oxidized Pt sites. Analogues of PtCl can be formed with other halide ions, and the present work focuses on a comparison of PtCl, PtBr, and PtI, where PtBr and PtI are understood to denote the same ethylenediamine/perchlorate compound, but with Br^- or I^- ions in place of the Cl^- ion, respectively.

Intrinsic localization of vibrational energy requires the presence of nonlinearity. In a simple view, if sufficient nonlinearity (manifest as anharmonicity) is present in a discrete lattice, then a delocalized vibrational excitation (small amplitude motions of a large number of lattice sites) can be stabilized by focusing into large amplitude motion on only a few lattice sites, since the large amplitude motion more effectively samples the anharmonicity. These considerations are independent of the actual source of the nonlinearity in the vibrational coordinates. Our earlier work on PtCl demonstrated that the interplay of electron delocalization interactions and electron−phonon coupling can lead to nonlinearity in vibrational degrees of freedom sufficient to drive the formation of ILMs.[3] In addition, since this nonlinearity arises from strong electron−phonon coupling, the use of resonance Raman spectroscopy as a means to study large-amplitude vibrational excitations (e.g., high overtones) suggests itself. Indeed, our study of ILMs in PtCl (isotopically pure in chloride isotopes) relied upon analysis of the anharmonic shifts of high overtones of the Raman-active Cl−Pt−Cl symmetric stretching mode and upon assignment of fine structure in high-overtone Raman spectra.[3] The latter arises from combination bands from states with overtone excitations of red-shifted localized modes in combination with fundamental excitations in more spatially extended motions.

An advantage of studying the platinum−halide linear chain materials is that nonlinearities can be chemically adjusted. For example, the substitution of Br^- or I^-ions for the Cl^- ion influences the relative strength of electron hopping and electron−phonon interactions.[15−17] In general, increasing electronic hopping interactions between sites leads to a greater degree of delocalization in both ground and excited electronic states, while strong electron−phonon coupling leads to localization of electronic states. More importantly for the present work, when the energy scale of electron−phonon coupling is comparable to electronic delocalization interactions, the strong coupling of vibrational and electronic degrees of freedom leads to nonlinear behavior in both. In electronic coordinates, these nonlinearities can appear as self-trapping processes such as those leading to self-trapped exciton and polaron formation and can be studied by techniques such as ultrafast time-resolved absorption. In the vibrational coordinates, one manifestation of the nonlinearities will be anharmonicities in the vibrational excitation energies, which can be studied by static vibrational spectroscopies. For PtCl, electron−phonon coupling and electronic interaction energies are indeed comparable, while the relative importance of electron−phonon coupling compared to electronic delocalization interactions decreases for PtBr and PtI. Thus one would expect the most nonlinearity in vibrational excitations in PtCl, less in PtBr, and the least in PtI.

We present an experimental study of the resonance Raman spectra across the PtCl, PtBr, PtI sequence. In agreement with the above considerations, we find that anharmonicity of the primary Raman-active mode in these materials varies, being strongest in PtCl, intermediate in PtBr, and completely absent in PtI. The presence of localized vibrational states (multiphonon bound states) is unambiguous in PtCl at 77 K, as also reported in our earlier work.[3] Such states are not observed in PtBr or PtI at 77 K, and there is only weak and somewhat ambiguous evidence of localized states in the mildly nonlinear PtBr even at 4 K. These results provide an important example of how nonlinearity leading to intrinsic localized mode (ILM) formation can be chemically tuned and will also relate to other recent studies that address the dynamics of trapping of electronic excitations (self-trapped exciton formation) in this same series of materials.

II. Experimental Section

Resonance Raman spectra in fundamental and overtone spectral regions were obtained with a SPEX 1702 single (1 m) spectrometer outfitted with an 1800 g/mm (SPEX 18001HD) grating and a liquid nitrogen cooled Princeton Instruments CCD-1152E/1 camera. For this high-resolution instrument, spectral resolutions of 0.44 and 0.26 cm^{-1}/pixel are obtained near 514.5 and 632.8 nm, respectively. Laser excitation sources (continuous wave) were a Coherent Innova 400 argon ion laser (514.5 nm) and a Uniphase 1144P HeNe laser (632.8 nm). Additional Raman excitation profile measurements, at lower spectral resolution, were made with a SPEX 1877 triple (0.6 m) spectrometer outfitted with a 1200 g/mm grating and a liquid nitrogen cooled CCD camera (Princeton Instruments CCD-1152 for red wavelength experiments or Photometrics PM512 with phosphor enhancement for blue wavelength experiments). For these additional measurements, various laser excitation sources were used including Ar-ion laser lines, a Spectra-Physics model 3900 Ti−sapphire (700−980 nm) pumped with a Spectra-Physics model 2040E Ar-ion laser, or a Coherent 590 dye laser pumped with the ultraviolet lines of a Spectra-Physics model 2040E Ar-ion laser. Calibrations of Raman spectra were performed by using low-intensity spectral calibration lamps, and peak positions in the Raman spectra were determined by fitting resolved spectral peaks to fit functions consisting of multiple symmetric peaks (e.g., Gaussians, Lorentzians) and linear sloping baselines. For the high signal-to-noise and relatively narrow fundamental and low overtone peaks, reproducibility of calibrations and of peak-fitting procedures from data set to data set indicate absolute uncertainties of ≤ 0.5 cm^{-1} in peak positions. For lower signal-to-noise and broader high overtone peaks, increased uncertainties in fitting peak positions range up to a few cm^{-1}.

For Raman measurements, single crystals were either suspended directly in liquid nitrogen contained in a transparent optical dewar (for 77 K measurements)[18] or were mounted in an Oxford Instruments continuous flow helium cryostat. In the latter case, the sample chamber was evacuated and backfilled with helium exchange gas maintained at slightly greater than ambient pressure, and the temperature was monitored by using a calibrated silicon diode. The long axis of the crystals (chain axis) was parallel with the polarization axis of the excitation beam (≤ 3 mW of incident laser power) that was focused to a ~ 200 μm spot at the crystal, and scattered light was collected in a backscattering geometry.

Diffuse reflectance spectra were measured at room temperature using a Perkin-Elmer Lambda 19 UV−Vis−NIR spectrophotometer with a Labsphere RSA-PE−19 reflectance spectroscopy accessory. Samples were ball milled in magnesium sulfate at $\approx 5\%$ w/w concentration, and were pressed between two glass microscope slides (Fisher) confined with a spacer. Diffuse reflectance spectra, obtained with pure ball-milled magnesium sulfate as a reference, were transformed to an absorption function using the Kubelka−Munk procedure.[19]

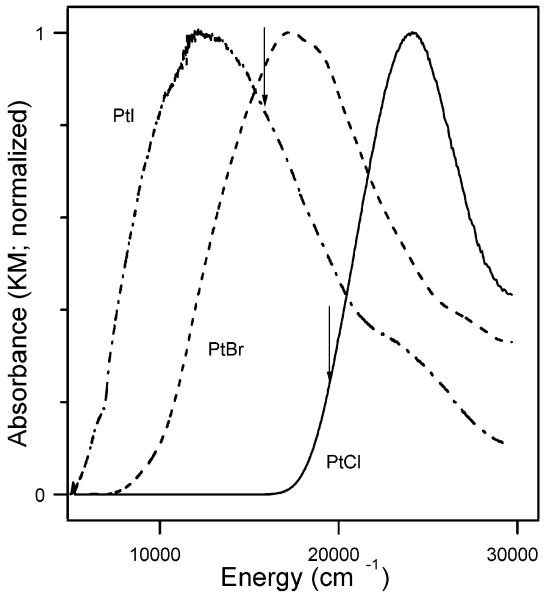

Figure 1. Room-temperature absorption spectra, presented as a Kubelka−Munk transform of diffuse reflectance data, for $[Pt(en)_2X_2]$-$[Pt(en)_2](ClO_4)_4$ where X = Cl (solid); X = Br (dotted); X = I (dot−dash). Spectra are normalized to the same peak value. From left to right, arrows correspond to 632.8 and 514.5 nm, which were the excitation wavelengths used for high-resolution resonance Raman spectroscopy in this work (632.8 nm for PtI and PtBr, 515.4 nm for PtCl).

$[Pt(en)_2X_2][Pt(en)_2](ClO_4)_4$ compounds for X = Cl, Br, and I were synthesized without chemical defects by a new procedure that involves maintaining the $[Pt(en)_2X_2]^{2+}$ concentration at very low levels (<1 mM) during crystallization. The general approach is to dissolve separately $[Pt(en)_2X_2](NO_3)_2$ (X = Cl, 0.0150 g, 0.0294 mmol; X = Br, 0.0176 g, 0.0294 mmol; X = I, 0.0204 g, 0.0294 mmol) and $[Pt(en)_2](NO_3)_2$ (0.0258 g, 0.0588 mmol), each in 6 mL of 1.2 M $HClO_4$, and to place the solutions into opposite tubes of a 30-mL H-tube flask. The solutions are then frozen and 10 mL of 1.2 M $HClO_4$ is layered over the frozen solutions to fill the H-tube cross piece. The H-tube flask is kept in darkness at 5 °C for 3−5 weeks, after which transparent red-orange needles and platelets (PtCl), lustrous green needles (PtBr), and lustrous gold needles (PtI) are harvested from only the tube rich in $[Pt(en)_2]^{2+}$. Complete synthetic procedures and compound characterization for the $[Pt(en)_2X_2](NO_3)_2$, $[Pt(en)_2]$-$(NO_3)_2$, and $[Pt(en)_2X_2][Pt(en)_2](ClO_4)_4$ (X = Cl, Br) are being published elsewhere, along with details of characterization of the defect-free nature of the materials prepared by the above procedure.[20] Details for *trans*-$[Pt(en)_2I_2](NO_3)_2$ are given here.[21]

III. Results

In the PtX series, resonance Raman spectra are dominated by scattering arising from ν_1, which is the symmetric Pt−halide stretching motion about the oxidized Pt site.[11,22] In a typical resonance Raman spectrum of PtX compounds, the ν_1 fundamental and several overtones are observed. Features corresponding to other totally symmetric motions (e.g., symmetric Pt−N stretch involving equitorial ligands) are also observed but are generally very weak relative to the ν_1 fundamental and first several overtones.

Diffuse reflectance spectra of defect-free PtCl, PtBr, and PtI are presented in Figure 1. The peak absorptions are found at 24 100 ± 180 cm^{-1} (2.99 eV; 415 nm), 17 250 ± 200 cm^{-1} (2.14 eV; 580 nm), and 12 900 ± 400 cm^{-1} (1.60 eV; 775 nm), respectively. Small distortions in the spectrum of PtI near 11 200 and 6900 cm^{-1} are due to weak water absorption peaks. High-resolution resonance Raman spectra of fundamental and overtone spectral regions were obtained by using excitation energies of 2.41 eV (514.5 nm) for PtCl and 1.96 eV (632.8 nm) for PtBr and PtI. These excitation energies are in resonance with the main optical absorption features of the compounds, as indicated in Figure 1.

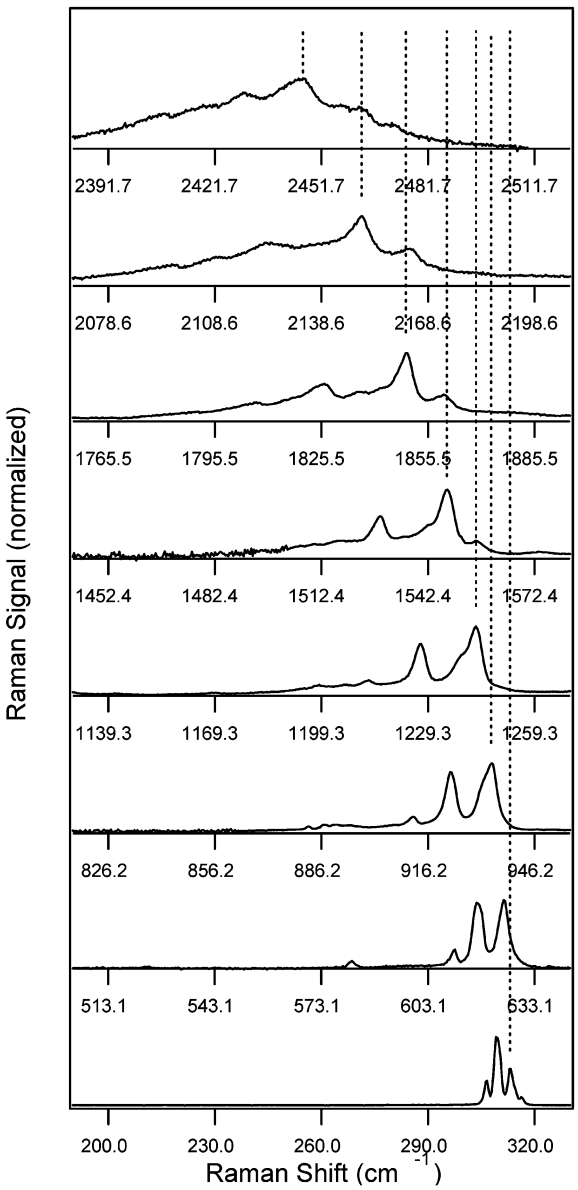

Figure 2. Fundamental and overtone Raman spectra, excited at 514.5 nm, of $[Pt(en)_2Cl_2][Pt(en)_2](ClO_4)_4$ at 77 K with natural Cl isotope abundance. Moving upward, each panel is offset by the appropriate integral multiple of 313.1 cm^{-1}, which is the frequency of the fundamental peak that evolves into isotopically pure $Pt^{35}Cl$ features at higher overtones (see text). All spectra have been scaled vertically to equal peak intensities of the highest intensity peak, which is the $Pt^{35}Cl$ peak for higher overtones.

Raman data for PtCl, measured at 77 K with 2.41 eV (514.5 nm) excitation, are presented in a slip-stack plot in Figure 2. The plot shows the ν_1 fundamental ($v = 0$ to $v = 1$ transition; lowest trace) and the first seven overtones. For presentation, the fundamental and overtone spectra have been scaled to equal peak intensities. In the actual raw spectra, the intensity of the seventh overtone is ≈345 times smaller than the fundamental. In the slip-stack plot, each overtone is presented with its horizontal axis translated to the left by a multiple of 313.1 cm^{-1}.

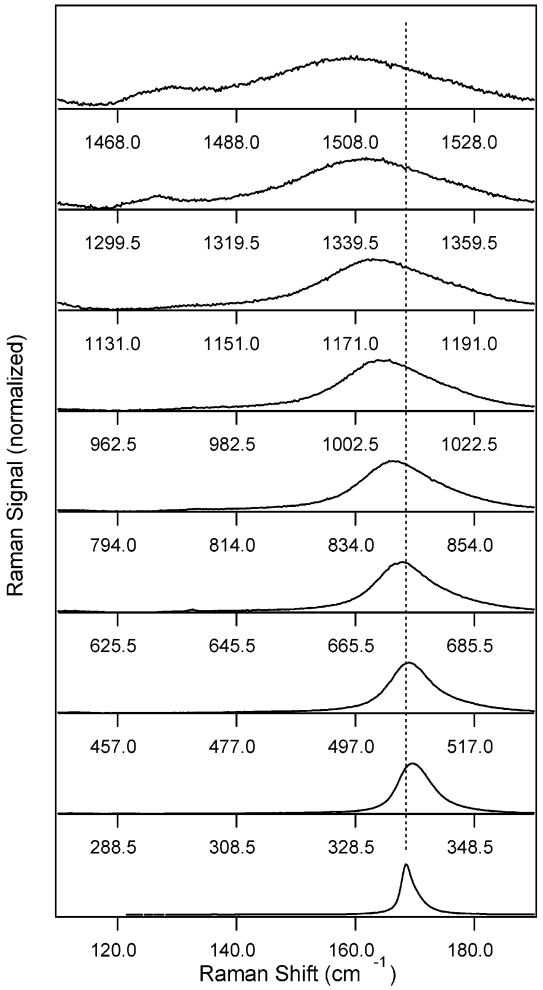

Figure 3. Fundamental and overtone Raman spectra, excited at 632.8 nm, of $[Pt(en)_2Br_2][Pt(en)_2](ClO_4)_4$ at 77 K presented as in Figure 2, but with 168.5 cm^{-1} offsets.

In such a plot, for a purely harmonic oscillator of frequency 313.1 cm^{-1}, the fundamental transition and all overtones would be aligned vertically. The sample studied here contained the natural abundance of chloride isotopes (75.8% ^{35}Cl, 24.2% ^{37}Cl), which leads to fine structure in the fundamental peak as previously observed.[22] In the current work, major peaks in the fundamental region are at 306.5, 309.1, 310.3, 313.1, 314.7, and 316.4 cm^{-1}. Prior modeling of this fine structure indicated that these peaks correspond to vibrations that extend over several unit cells of the material with different statistical isotopic patterns.[22−25] Similarly, the first overtone fine structure also corresponds to a set of isotopically mixed vibrations that may extend over more than one $PtCl_2$ unit.[25] At the second overtone, a simple three-peak pattern is observed, and the peak heights are in the ratio of ≈1:6.5:8.7. As discussed below, these intensities suggest that the second overtone spectrum corresponds to excitation of single $PtCl_2$ units with a statistical distribution of isotopes. Thus, the highest frequency peak (934 cm^{-1}) in the second overtone spectrum corresponds to the symmetric stretch of a $^{35}Cl-Pt-^{35}Cl$ unit. In this and higher overtone traces, the evolving position of this peak is tracked by the vertical lines in Figure 2, and the red shift of this feature corresponds to the anharmonicity analyzed below.

The results of a similar experiment for PtBr at 77 K, excited at 1.96 eV (632.8 nm), are presented in Figure 3. The fundamental and first eight overtones of ν_1 are shown. For reference, here the intensity of the eighth overtone prior to scaling was ≈130 times smaller than the fundamental. The fundamental is observed as a single peak at 168.5 cm^{-1}. An appropriate multiple of this value is used to offset the horizontal axis for each overtone region, resulting in the slip-stack plot shown. The peak position of the fundamental is indicated by the vertical dashed line. Small anharmonicities are apparent from the shifts of higher overtone peaks away from this line and are analyzed below. No fine structure is resolved, either in the fundamental or any of the overtones. To explore whether the modest anharmonicities in PtBr might lead to observable localized modes if random thermal excitations are greatly reduced, the fundamental and first 11 overtone spectra were also measured at 4 K. These spectra, also scaled to equal peak intensities, are shown in Figure 4, and were also obtained by using 1.96 eV (632.8 nm) excitation. At 4 K, the fundamental peak (lowest trace) is observed at 166.6 cm^{-1}, and multiples of this value are used to generate the slip-stack plot in Figure 4. The development of anharmonicity is similar to that seen at 77 K. No clear combination band evidence is observed to indicate the formation of intrinsically localized modes. However, at very

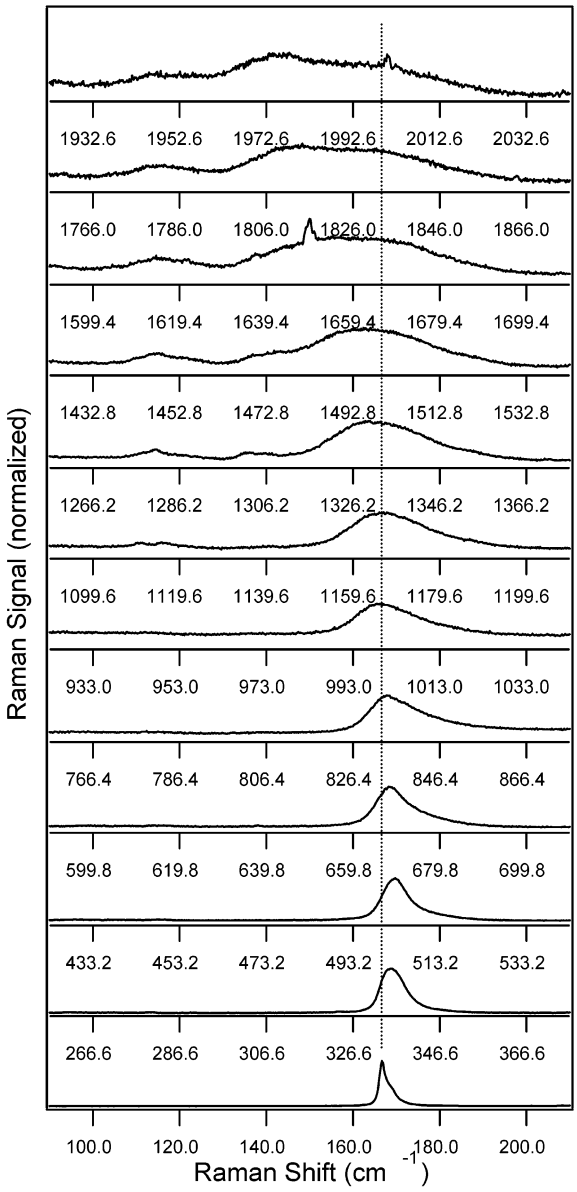

Figure 4. Fundamental and overtone Raman spectra, excited at 632.8 nm, of $[Pt(en)_2Br_2][Pt(en)_2](ClO_4)_4$ at 4 K presented as in Figure 2, but with 166.6 cm^{-1} offsets.

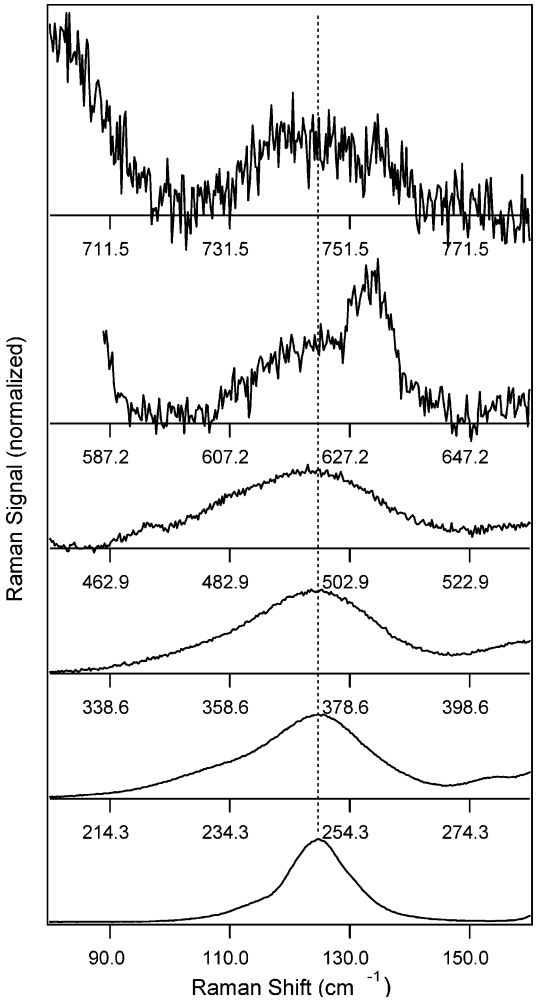

Figure 5. Fundamental and overtone Raman spectra, excited at 632.8 nm, of $[Pt(en)_2I_2][Pt(en)_2](ClO_4)_4$ at 77 K presented as in Figure 2, but with 124.3 cm^{-1} offsets.

high overtone levels (ninth through eleventh overtones; top three traces of Figure 4), there is some poorly resolved broad structure observed in the ν_1 overtone region, which is discussed below. Note that the weak, very sharp, features at 1649 and 2001 cm^{-1} are due to plasma lines from the excitation laser.

The fundamental and overtone resonance Raman spectra measured for PtI at 77 K, with excitation at 1.96 eV (632.8 nm), are presented in Figure 5. Again, all spectra were scaled to equal peak intensities of the ν_1 fundamental and overtones. The fall off of intensity with increasing overtone level is much sharper for PtI than for PtBr or PtCl, and signal-to-noise limitations preclude study of overtones beyond the fifth. For reference, the fifth overtone is ≈380 times smaller than the fundamental prior to scaling. Thus, other weakly allowed low-frequency Raman-active modes with intensities comparable to or greater than the ν_1 progression are evident throughout the slip-stack plot, such as the peak at ≈631 cm^{-1}. Similar features are also present in the PtBr and PtCl spectra, but are substantially weaker than the dominant ν_1 progression in those cases. For excitation at 1.96 eV, peak fitting yields the fundamental to be at 124.3 cm^{-1}, and appropriate multiples of this value are used to shift the horizontal axis for the overtones. Within experimental resolution, there is no observed shift of the overtone peaks away from the harmonic (linear) value.

Results of analysis of the shifts presented above can be collected in a single plot, in which the relative shift, r_n, is plotted versus the final number of quanta, n, for the fundamental and

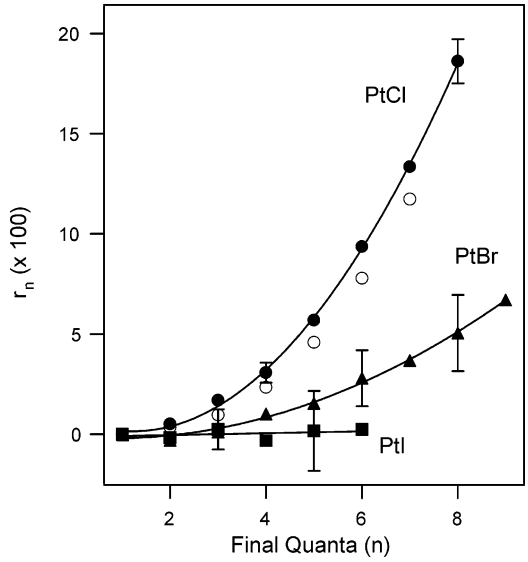

Figure 6. (a) Shifts of the 77 K overtone peaks from harmonic responses, normalized by the fundamental frequency, as a function of final quanta of ν_1 vibrational energy for $[Pt(en)_2X_2][Pt(en)_2](ClO_4)_4$: X = Cl (solid circles); X = Br (solid triangles); X = I (solid squares). For PtCl, the ^{35}Cl component of isotopically resolved fine structure is tracked (see text). Quadratic (PtCl and PtBr) and linear (PtI) best fits are shown as solid lines. Open circles are shifts for isotopically pure $Pt^{35}Cl$ material at 12 K (from ref 3). For two representative points of each 77 K data set, error bars were calculated from error propagation analysis of uncertainties in fundamental peak positions and overtone peak positions. Largest relative errors are found for high overtones of PtI. This reflects both the low signal-to-noise of these spectra (see Figure 5) and the low frequency of the ν_1 fundamental of PtI, which amplifies the relative importance of small uncertainties in absolute position.

each overtone. The relative shift is calculated as $r_n = (n\omega_R - \omega_R^{(n)})/\omega_R$, where $\omega_R^{(n)}$ is the observed frequency of the multiphonon state with n quanta and $\omega_R = \omega_R^{(1)}$, the fundamental frequency. For PtCl, $\omega_R = 313.1$ cm^{-1}; for PtBr, $\omega_R = 168.5$ cm^{-1}; and for PtI, $\omega_R = 124.3$ cm^{-1}. As already noted, in the case of PtCl the analysis here is focused on the resolved $^{35}Cl-Pt-^{35}Cl$ peak, but a similar analysis can also be performed for any of the resolved features corresponding to different isotope patterns. The shifts as a function of number of final quanta of excitation energy are presented in Figure 6 for PtCl (resolved ^{35}Cl peak), PtBr, and PtI. The red shift (nonlinearity) of the vibration is strongest for PtCl, modest for PtBr, and nonexistent for PtI. For comparison, also shown in Figure 6 is the red shift for isotopically pure PtCl (taken from the data presented in Figure 4 of Swanson et al.[3]). The red shift in isotopically pure PtCl is systematically slightly smaller than in the isotopically disordered natural abundance material, a point that is discussed below.

For each material several additional Raman experiments at different excitation wavelengths spanning the optical absorption bands were performed to check for possible excitation wavelength dependence in the ν_1 fundamental and overtone peak positions. For materials synthesized by the procedure reported here, no variation in the frequency of ν_1 is observed for PtCl with excitation between 1.64 eV (756.0 nm) and 2.94 eV (421.7 nm), nor for PtBr with excitation between 1.32 eV (939.3 nm) and 1.96 eV (632.8 nm). At low temperature, photoexcitation of PtBr at higher energies, such as 2.33 eV (532 nm) and above, leads to formation of several new photoinduced Raman modes at higher energies than the fundamental peak. This effect has been previously observed.[26] Also, for PtI, the frequency of ν_1 is observed to vary with excitation wavelength for wavelengths

SCHEME 1: Schematic Structure along the Chain Axis of PtX Materials[a]

…-X—$Pt^{+(3+\delta)}$—X-----$Pt^{+(3-\delta)}$-----X—$Pt^{+(3+\delta)}$—X-----$Pt^{+(3-\delta)}$-----X—$Pt^{+(3+\delta)}$—X-…

[a] The strength of the charge density wave corresponds to the magnitude of δ. The halide sublattice is distorted toward the oxidized metal site, leading to the presence of both short and long metal−halide bond lengths. The ratio of the short to long bond lengths varies from ≈0.74 for X = Cl, to ≈0.83 for X = Br, to ≈0.89 for X = I. For clarity, neither ethylenediamine transverse ligands nor chain counterions are represented.

between 939 nm (1.32 eV) and 632.8 nm (1.96 eV), which was the range studied in the present work. This result is also consistent with previous work.[11] Through this range, the fundamental peak frequency increases continuously with increasing excitation energy and varies from 110 cm^{-1} at 1.32 eV to 124 cm^{-1} at 1.96 eV. In all cases, however, the position of the overtone peaks of ν_1 tracked with the fundamental position in PtI, yielding the same overall harmonic behavior as shown in Figures 5 and 6.

IV. Discussion

Overview. The structures of halide-bridged mixed-valence platinum compounds have been previously studied and tabulated.[13] Due to the commensurate CDW formation and Peierls distortion, there are alternating short and long platinum−halide bond lengths along the chain axis. The long and short bond lengths, respectively, for low-temperature monoclinic phases of the PtX series studied here are 3.122, 2.319 Å for X = Cl, 3.001, 2.484 Å for X = Br, and 3.048, 2.712 Å for X = I.[14,27] The quasi-one-dimensional structure of these compounds is illustrated in Scheme 1. The structures vary systematically, with the halide sublattice being most distorted in the X = Cl material, as judged by the ratio of short and long Pt−X bond lengths. The structural distortion reflects a competition between intersite electronic coupling and electron−phonon coupling. The former favors a delocalized symmetric material and the latter favors local geometrical distortions that stabilize alternating oxidized and reduced metal sites. For X = Br and I, electronic delocalization is enhanced by interaction of Pt d_{z^2} orbitals with the halide $4p_z$ and $5p_z$ orbitals, respectively, while for X = Cl, the halide $3p_z$ orbitals participate much less strongly in mediating metal−metal electronic interactions.[16] Thus, all other factors being equal, electronic coupling arguments alone lead to a predicted increase in delocalization and a corresponding decrease in ground-state structural distortion, as X is varied from Cl to Br to I.

Along these lines, both theoretical and experimental considerations indicate that the strength of electron−phonon interactions relative to electronic delocalization interactions is strongest for PtCl, intermediate for PtBr, and weakest for PtI. Theoretically, this trend has been explored in numerous models of varying degrees of sophistication and is found to be needed for successful prediction of electronic, structural, and optical properties of the materials.[15−17] Experimentally, the influence of electron−phonon coupling relative to electronic delocalization interactions can also be approximately estimated from structural and spectroscopic data. Using the halide mass and the observed frequency of the Raman fundamentals, the root-mean-square displacement of the ground-state vibrational wave function corresponding to the motion of a halide ion between two metal ions can be estimated. This result is 0.039, 0.035, and 0.033 Å for chloride, bromide, and iodide, respectively. The distortion of the short Pt−X bond length away from the symmetric structure, divided by this ground state wave function rms value, provides a dimensionless parameter reflecting the geometric displacement on a halide ion between the charge disproportionated ground state and an excited electronic state in which charges are equally distributed along the chain. This dimensionless displacement is often referred to as Δ, and its square is proportional to a Huang−Rhys factor, S, associated with linear vibronic coupling ($S = \Delta^2/2$). The Huang−Rhys factor times the mode energy ($S\hbar\omega$) provides an estimate of the energy scale associated with local lattice distortions arising from electron−phonon coupling. For the Pt−X series, this calculation yields energy scales of ≈2.0 eV (16 400 cm^{-1}) for PtCl, ≈0.6 eV (4600 cm^{-1}) for PtBr, and ≈0.2 eV (1600 cm^{-1}) for PtI. Since the degree of charge disproportionation varies for the three materials, these estimates of energy scales associated with the observed structural distortions actually reflect the interplay between electron−phonon coupling and electronic delocalization. Also, since they rely upon linear electron−phonon coupling only, they are only very crude estimates of the relevant energy scales, particularly for PtCl.[13] Nevertheless, qualitatively, these arguments based on simple experimental considerations also lead to the conclusion that the influence of electron−phonon coupling relative to electronic delocalization is strong for the chloride material. In contrast, the influence of this coupling is less for the bromide system and small for the iodide material.

From all the above considerations, one would expect that PtI would have a nearly linear Raman spectrum. The limited role of electron−phonon coupling should also lead to PtI having only modest overtone strength in its Raman spectrum, as is observed. In contrast, the Raman spectrum PtCl should be highly nonlinear. Here, the coupling energy between the electronic excitations and vibrations is comparable to the energy of an electronic excitation. The effective potential energy surfaces for vibrations will be highly perturbed from a simple harmonic oscillator, and indeed, nonlinearities may be so large that separability of the vibrational and electronic coordinates is not appropriate at all.[3,9,16,17] Both anharmonicities and substantial strength in overtone transitions should be observed, consistent with experimental results. PtBr should show intermediate behavior, and experimentally, PtBr demonstrates strong intensity in its ν_1 overtone progression but has very little anharmonicity.

PtCl Analysis. In nonlinear materials, a qualitative expectation is that larger amplitude vibrational motions will more effectively sample the nonlinear or anharmonic character of the dynamics. Thus, in a Raman scattering experiment, the effects of nonlinearities in the vibrational motion, including stabilization of localized excitations, should become increasingly apparent for higher overtone excitations. Several observable indications of localization phenomena are possible, including fine structure due to isotopic distributions, red shifts corresponding to the stabilization of localized states, and the appearance of combination bands involving combined excitation of localized high overtone states and more delocalized states with fewer quanta of excitation. PtCl, the most nonlinear material studied here, demonstrates all of these phenomena.

Isotopic Fine Structure. For PtCl at 77 K, the fundamental peak (lowest trace of Figure 2) has resolved fine structure that corresponds to vibrational modes extending over several unit cells with different statistical distributions of ^{35}Cl and ^{37}Cl isotopes.[22,25] Since these modes are already partially localized by the isotopic disorder even for the fundamental excitation, to truly explore intrinsic localization phenomena in the absence of such disorder, study of isotopically pure PtCl is required. Relevant results on both the ^{35}Cl and ^{37}Cl isotopically pure PtCl materials have been previously published by our co-workers

and us.[3] However, the focus of the current work is comparison of the PtX series. As is discussed below, the development of nonlinearities in the natural abundance PtCl material is very similar to that in the isotopically pure material, so the current work uses the easier to synthesize and substantially cheaper natural abundance PtCl material.

The positions observed here for the fine structure peaks in the fundamental spectrum are systematically about 1 cm^{-1} higher than those reported by Love et al.[22] However, the current experiments were performed at 77 K, while those reported previously were performed at 13 K, which could easily lead to a shift of this small amount.[14] Based on matching the similar intensity patterns of the two spectra, the peak we observe at 313.1 cm^{-1} corresponds directly to the peak observed by Love et al. at 312.0 cm^{-1}, which in turn is assigned as arising from a segment of chain that consists of several adjacent $Pt^{35}Cl_2$ units (with, of course, intervening reduced Pt^{2+} sites). Essentially, this peak corresponds to the Raman scattering from a small segment of pure ^{35}Cl chain. Lower intensity, higher frequency, features, such as the one we observe at 316.4 cm^{-1} (315.4 cm^{-1} in the 13 K spectrum of Love et al.), are assigned as arising from a $Pt^{35}Cl_2$ unit bounded by $Pt^{35}Cl^{37}Cl$ units.[22] Lower frequency peaks contain contributions from 35−37 and di-37 units. Based on these assignments, the peak at 313.1 cm^{-1} represents the best choice of fundamental frequency for an analysis of the natural abundance material that will focus on $Pt^{35}Cl$ features. This peak arises from a segment of chain that allows partial delocalization of the Pt−^{35}Cl mode and also closely matches the frequency of the isotopically pure $Pt^{35}Cl$ material (also seen at 312 cm^{-1} at 13 K)[3].[22] While higher frequency peaks also have $Pt^{35}Cl$ character, they most nearly represent modes corresponding to a $Pt^{35}Cl_2$ defect in a chain of $Pt^{35}Cl^{37}Cl$ units. In this case, the fundamental already shows a strong artificial degree of localization induced by isotopic disorder, which would greatly complicate any analysis.

An evolution of spectral line shapes that corresponds to increasing localization of the vibrational state is already apparent in moving from the fundamental to the first overtone (second trace from bottom in Figure 2) and becomes even more evident at the second overtone (third trace from bottom in Figure 2). For a vibrational excitation localized onto a single $PtCl_2$ unit, a statistical distribution of isotopes would lead to a triplet feature with relative intensities of 1:6.3:9.8 for the $Pt^{37}Cl_2$, $Pt^{35}Cl^{37}Cl$, and $Pt^{35}Cl_2$ contributions, respectively. As just discussed, this is not the observed structure in the fundamental region. However, a three-peak structure begins to develop in the first overtone and is fully evident in the second overtone, where the peak heights are 1:6.5:8.7. Isotopic abundances that would lead to this observed intensity distribution can be calculated independently from either the 1:6.5 or the 1:8.7 ratios. These calculations result in 23.5%(^{37}Cl)/76.5%(^{35}Cl) and 25.3%(^{37}Cl)/74.7%(^{35}Cl), respectively, which narrowly bracket the expected 24.2%(^{37}Cl)/74.8%(^{35}Cl). Thus, the observed intensity pattern of the second overtone is judged to be in good agreement with expectations for a vibration localized on a single $PtCl_2$ unit, and so the evolution of the fine structure provides clear evidence for the spatial focusing of vibrational excitations as the amplitude of the motion increases. The present results also show that this focusing still occurs at 77 K, as well as at the lower temperatures (12 K) described briefly (but not presented) in our previous work.[3] The same general intensity pattern corresponding to a single $PtCl_2$ unit persists at higher overtone levels, but detailed analysis of the intensity patterns becomes increasingly difficult due to lower signal-to-noise, increased peak widths, and the appearance of additional fine structure due to combination bands (see below).

Red Shifts. Tracking the deviation of overtone energies from values expected for purely harmonic behavior yields the anharmonicity. In Figure 6, we demonstrate that the anharmonicity of $Pt^{35}Cl_2$ vibrations within natural abundance PtCl is quite similar to the previously studied isotopically pure compound but is slightly more developed at each quanta of excitation. This occurs even though the natural abundance data presented here were obtained at 77 K, while the isotopically pure data were obtained at ≈12 K. This result suggests that the basic nonlinearities and localization phenomena are the same for the two materials but that the peaks being tracked in the natural abundance material correspond to a chain segment in which the fundamental excitation is very slightly confined by isotopic disorder. The confinement due to isotopic disorder has the effect of marginally increasing the observed red shift for a particular vibrational quantum level or, equivalently, shifting the development of a particular value of the red shift to approximately one-half quanta lower level in the natural abundance material.

Combination Bands. Another signature of localization is the appearance of bands that can be assigned to localized excitations appearing in combination with lower quanta, more delocalized states. These combination bands become most apparent in a slip-stack plot with slips at the fundamental frequency. In such a plot, when moving from the nth overtone to the $(n+1)$th overtone, features that correspond to the nth overtone and to the nth overtone combined with one quanta of fundamental excitation will be vertically aligned. There are a number of examples evident in the PtCl slip-stack plot shown in Figure 2. For example, on moving from the fourth overtone (five overall quanta of energy; fifth trace from bottom) to the fifth overtone, it is apparent that the dominant peak in the fourth overtone leads to a satellite peak in the fifth overtone region that involves adding one additional quanta at the fundamental frequency (313.1 cm^{-1}). In addition, the fifth overtone has a further red-shifted peak corresponding to all six quanta of energy residing in the localized state. Similar examples can be found in every case from the third overtone upward. These combination bands are analogous to similar features assigned in direct absorption overtone spectra of molecules with local mode behavior.[28] It is interesting to note that, when tracking the feature derived from the $Pt^{35}Cl_2$ oscillator, the combination bands that appear involve excitation of that oscillator in combination with the more extended 313.1 cm^{-1} fundamental mode that corresponds to an excitation on a ^{35}Cl dominated chain segment. A similar analysis focusing on other isotopic components of the second overtone feature, for example, the mixed $^{35}Cl-^{37}Cl$ species, leads to similar results involving combination bands with fundamental frequencies that correspond to mixed isotopic chain compositions. All of these combination bands, involving different localized and fundamental isotopic patterns, contribute to the large number of peaks observed at red-shifted positions in higher overtones, but analysis along the lines indicated here leads to definitive assignments for nearly every resolvable peak in all the overtone spectra.

PtBr Analysis. In PtBr, the relative strength of electron−phonon coupling versus electronic delocalization interactions is decreased from PtCl. Thus, the material is expected to exhibit much more delocalized electronic behavior, and the influence of electron−phonon coupling should be much weaker. These considerations suggest that PtBr vibrations should be substan-

tially closer to harmonic. The results presented above are consistent with this view. For example, at 77 K (Figures 3 and 6), the overall anharmonicity observed for PtBr is much smaller than that observed for PtCl. Even at very high overtones, the purely harmonic frequency (vertical line in Figure 3) is well within the peak width of the slightly red-shifted overtone band. In addition, no evidence of resolved fine structure is observed, either due to the appearance of combination bands or due to isotopic effects in the natural abundance PtBr material.

This latter point requires some discussion. In all the PtX materials studied here, multiple Pt isotopes are present, but the relative mass differences of Pt isotopes are quite small, and further, Pt motion does not contribute to the Raman-active ν_1 mode. Thus, observation of any Pt isotope splitting or Pt-induced localization phenomena in the ν_1 mode would not be expected. In contrast, Br isotopes could lead to resolvable splittings if strong localization occurred. The two stable Br isotopes are ^{79}Br (50.7%) and ^{81}Br (49.3%). Since $(81/79)^{1/2} = 1.0126$, approximately 1.26% splittings might be expected for isolated bromide stretching motions. For a mode at 168 cm^{-1}, this splitting would correspond to 2.1 cm^{-1}, which would be observable. However, if vibrational states in a material are highly extended, then isotopic splittings tend to be unobservable. Full exploration of this point for PtBr would require realistic numerical simulations of the PtBr lattice with statistical isotope distributions and is not further pursued here. Qualitatively, however, the lack of observable fine structure associated with isotope patterns in PtBr, which is also true for the infrared active modes,[23] is further evidence that the vibrational excitations in this material are substantially delocalized.

Because the fundamental frequency of PtBr is lower than that of PtCl, the role of thermal excitations in destabilizing local mode states should be carefully considered. This is particularly true since PtBr does demonstrate some anharmonicity (in contrast to PtI). The spectra of PtBr overtones at liquid helium temperatures were carefully examined (Figure 4). Overall, the results at 4 K are very similar to those at 77 K. The fundamental frequency shifts slightly at the decreased temperature,[14] from 168.5 to 166.6 cm^{-1}, and this latter value is used to generate the slip-stack plot shown in Figure 4. At 77 K and especially at 4 K there are very small shifts of the first few overtones to slightly higher energy than would be expected for purely harmonic behavior. These shifts are reproducibly obtained but are close to the resolution of the spectral data. Further analysis of these small effects is not attempted here.

While the development of the anharmonicity is quite similar at 4 K to that found at 77 K, higher overtone data were obtained at the lower temperature. In the 9th, 10th, and 11th overtones (top three traces of Figure 4), there is some very poorly resolved fine structure that appears. For example, in the 10th overtone, there is a peak at $\approx$1811 cm^{-1} and a poorly resolved subpeak at $\approx$1834 cm^{-1}. Such features could result from combination bands, as discussed for higher overtones of PtCl (see Figure 2, and Figures 2 and 3 of Swanson et al.[3]), in which case they would indicate the onset of localization. However, other sources for these particular features in the PtBr spectra cannot be ruled out. For example, there are weak modes other than ν_1 observed at $\approx$1115 cm^{-1} and $\approx$1302 cm^{-1} (seventh and eighth traces from bottom, respectively, in Figure 4). Each of these modes then appears in combination with fundamental and low overtone excitations in ν_1 in all higher traces. In particular, the mode that originates near 1302 cm^{-1}, in combination with two, three, and four quanta of excitation in ν_1, could contribute to the observed poorly resolved structure at higher overtones.

Overall, uncertainties in assignment of the weak fine structure, and the fact that the red shifts of ν_1 overtones are of similar magnitudes to their peak widths, even at 4 K, preclude the unambiguous identification of localization phenomena in PtBr. A definite conclusion is that no spectroscopic evidence of localized vibrational excitations in PtBr exists for up to nine quanta of excitation at either 77 or 4 K. At higher quanta excitation at 4 K, there are only very ambiguous indications of localization. Clearly, the reduction of the importance of electron−phonon coupling relative to electronic delocalization interactions in PtBr compared to PtCl greatly reduces the nonlinear nature of the vibrational excitations in the former.

PtI Analysis. As already discussed, PtI is characterized by an even smaller strength of electron−phonon coupling relative to electronic delocalization interactions than that of PtBr. Thus, PtI should be even more clearly in the limit of full electronic delocalization (consistent with its behavior as a low band-gap semiconductor[16]), and the anharmonicities introduced by the competition of electronic delocalization interactions and electron−phonon coupling should be minimal. Indeed, the results reported above are fully consistent with this view. Within experimental resolution, the 77 K Raman spectra of ν_1 in PtI are fully harmonic through the first five overtones (Figures 5 and 6). Further, the overall strength of the high overtone scattering is sharply reduced relative to that observed with either PtBr or PtCl. Finally, of course, there is no observable fine structure that could indicate the presence of combination bands involving vibrationally localized multiquanta states. Because of the harmonic response and the lack of overtone scattering strength, the behavior of PtI at lower temperatures was not further explored. Overall, we conclude that the Raman-active vibrational excitations of PtI are harmonic (linear) and delocalized.

Relevance to Electronic Dynamics in PtX Materials. The studies reported here indicate that the propensity for formation of localized vibrational states in the PtX series varies systematically. PtCl forms well-defined multiquanta bound states that reflect intrinsic localization driven by the interplay of electron−phonon coupling and electronic delocalization. PtBr demonstrates some anharmonicity, but the nonlinearity is not sufficient to lead to the unambiguous observation of stable highly localized vibrations. PtI demonstrates no indication of either stable localized vibrational states or anharmonic responses.

As mentioned above, the formation of a self-trapped exciton following electronic excitation of a delocalized electron−hole pair is a process also governed by the interplay of electronic interactions and electron−phonon coupling. Thus, it is interesting to compare the present results with recent studies of the dynamics of exciton self-trapping in PtX materials. Dexheimer et al. recently reported ultrafast time-resolved experiments exploring the self-trapping process in PtBr and PtCl.[29,30] These experiments used excitation pulses short relative to the vibrational period of fundamental Raman-active phonons. The subsequent impulsive excitation leads to both excited electronic state dynamics and coherent phonon dynamics. Changes in the absorption spectra following photoexcitation can be used to monitor formation of the self-trapped exciton state, and correlated changes in the spectra arising from the coherent vibrational states can be used to identify excited-state vibrational motions that lead to the self-trapped state. Thus, both the time scale for formation of the self-trapped state and the frequency of the vibrational motion in the excited electronic state that carries the system into the self-trapped exciton state can be determined. Up to 40% softening of the Raman active coordinate was observed in the excited electronic state for both PtBr and

PtCl, which is one manifestation of the strength of electron−phonon coupling in both systems. The overall speed of the self-trapping process was observed to be faster for PtCl than for PtBr,[30] which could be consistent with the view that the relative strength of electron−phonon coupling compared to electronic delocalization factors is stronger for PtCl. However, in both materials, the dynamics of the self-trapping process are similar to a single vibrational period, in line with a barrierless trapping mechanism in a quasi-one-dimensional system. Thus, while these results are qualitatively consistent with the trends explored in the present work, quantitative theoretical connections between the time-resolved studies and the vibrational nonlinearities explored in the present work remain to be fully developed.

In fact, when taken together, the present work and the time-resolved studies provide a relatively complete experimental picture of the nature of vibrational and electronic excitations, and their coupled dynamics, in the PtX series. These data address localization and trapping phenomena in low-dimensional materials as a function of electron delocalization interactions and electron−phonon coupling strengths and thus provide a general testing ground for theoretical analysis of such processes. Numerous challenges continue to exist in obtaining a detailed theoretical treatment. These include developing a full dynamical description of strongly coupled electronic and vibrational states whose spatial extent varies with time, exploring how such dynamics are manifest in time-resolved spectroscopic measurements, and quantitatively understanding how electronic state dynamics and localization processes influence resonance Raman scattering and other nonlinear spectroscopies in such systems. On the other hand, an opportunity exists to use the set of experimental static and time-resolved linear and nonlinear spectroscopic results on the entire series of PtX materials to benchmark the development of appropriate theoretical descriptions. Such treatments would increase general understanding of how electronic delocalization and electron−phonon coupling interactions influence the electronic and optical responses of a variety of low-dimensional materials.

V. Summary and Conclusions

A systematic study of the resonance Raman spectra of a series of halide-bridged mixed-valence transition-metal compounds has been presented. In the series studied here, the degree of material nonlinearity is controlled by the relative strengths of electron−vibration coupling and electronic delocalization interactions. When the strengths of these interactions are comparable, as in PtCl, the strong coupling between the vibrational and electronic excitations leads to complex nonlinear responses in both vibrational and electronic degrees of freedom. In the case of PtCl, one observes that Raman scattering into high overtone excitations creates states that are spatially localized, and combination states of localized high overtone states with more delocalized vibrational fundamentals are found. The localized multiquanta bound states, or intrinsically localized modes, are formed since the strongly coupled electronic/vibrational problem leads to large vibrational anharmonicities, which, in turn, stabilize localized vibrational states. PtBr, which is expected to have much less nonlinearity in its vibrational degrees of freedom, demonstrates small anharmonicity and only ambiguous evidence of stable localized vibrational states. Finally, PtI yields Raman spectra that are fully consistent with linear, delocalized, vibrations.

The present work contributes to an increasingly complete set of data addressing vibrational and electronic excitations in the PtX series. While the qualitative discussion developed here leads to a consistent view of the factors that govern the excited-state structure and dynamics, a fully detailed quantitative theoretical description of how the coupling of electronic and vibrational excitations determines material properties remains incomplete, both for PtX materials and other low-dimensional electronic materials in which similar effects are important. Obtaining such an understanding that is consistent with the full range of available experimental results remains an area of active effort.

Acknowledgment. We thank our colleagues A. R. Bishop, G. Kalosakas, S. L. Dexheimer, and B. I. Swanson for useful discussions, and we acknowledge support from the Department of Energy, Office of Science and the Los Alamos National Laboratory LDRD program.

References and Notes

(1) (a) Sievers, A. J.; Takeno, S. *Phys. Rev. Lett.* **1988**, *61*, 970. (b) Page, J. B. *Phys. Rev. B* **1990**, *41*, 7835.

(2) (a) Kiselev, S. A.; Sievers, A. J. *Phys. Rev. B* **1997**, *55*, 5755. (b) Hizhnyakov, V.; Nevedrov, D.; Sievers, A. J. *Physica B* **2002**, *316*−*317*, 132. (c) Rössler, T.; Page, J. B. *Phys. Rev. B* **2000**, *62*, 11 460. (d) Peyrard, M.; Farago, J. *Physica A* **2000**, *288*, 199. (e) Wang, W. Z.; Gammel, J. T.; Bishop, A. R.; Salkola, M. I. *Phys. Rev. Lett.* **1996**, *76*, 3598. (f) Wang, W. Z.; Bishop, A. R.; Gammel, J. T.; Silver, R. N. *Phys. Rev. Lett.* **1998**, *80*, 3284. (g) MacKay, R. S.; Aubry, S. *Nonlinearity* **1994**, *7*, 1623. (h) Aubry, S. *Physica D* **1997**, *103*, 201. (i) Flach, S.; Willis, C. R. *Phys. Rep.* **1998**, *295*, 181. (j) Flach, S.; Kladko, K.; MacKay, R. S. *Phys. Rev. Lett.* **1997**, *78*, 1207.

(3) Swanson, B. I.; Brozik, J. A.; Love, S. P.; Strouse, G. F.; Shreve, A. P.; Bishop, A. R.; Wang, W. Z.; Salkola, M. I. *Phys. Rev. Lett.* **1999**, *82*, 3288.

(4) (a) Schwarz, U. T.; English, L. Q.; Sievers, A. J. *Phys. Rev. Lett.* **1999**, *83*, 223. (b) English, L. Q.; Sato, M.; Sievers, A. J. *J. Appl. Phys.* **2001**, *89*, 6707. (c) Sato, M.; English, L. Q.; Hubbard, B. E.; Sievers, A. J. *J. Appl. Phys.* **2002**, *91*, 8676.

(5) (a) Edler, J.; Hamm, P. *J. Chem. Phys.* **2002**, *117*, 2415. (b) Edler, J.; Hamm, P.; Scott, A. C. *Phys. Rev. Lett.* **2002**, *88*, 067403.

(6) (a) Careri, G.; Buontempo, U.; Galluzzi, F.; Scott, A. C.; Gratton, E.; Shyamsunder, E. *Phys. Rev. B* **1984**, *30*, 4689. (b) Eilbeck, J. C.; Lomdahl, P. S.; Scott, A. C. *Phys. Rev. B* **1984**, *30*, 4703. (c) Christiansen, P. L., Scott, A. C., Eds. *Davydov's Soliton Revisited: Self-Trapping of Vibrational Energy in Protein*; Plenum Press: New York, 1990; Section IV.

(7) (a) Lehmann, K. *Annu. Rev. Phys. Chem.* **1994**, *45*, 241. (b) Crim, F. F. *Annu. Rev. Phys. Chem.* **1993**, *44*, 397. (c) Child, M. S.; Halonen, L. *Adv. Chem. Phys.* **1984**, *57*, 1. (d) Child, M. S. *Acc. Chem. Res.* **1985**, *18*, 45. (e) Henry, B. R. *Acc. Chem. Res.* **1977**, *10*, 207.

(8) (a) Trías, E.; Mazo, J. J.; Orlando, T. P. *Phys. Rev. Lett.* **2000**, *84*, 741. (b) Binder, P.; Abraimov, D.; Ustinov, A. V.; Flach, S.; Zolotaryuk, Y. *Phys. Rev. Lett.* **2000**, *84*, 745. (c) Trías, E.; Mazo, J. J.; Brinkman, A.; Orlando, T. P. *Physica D* **2001**, *156*, 98. (d) Schuster, M.; Binder, P.; Ustinov, A. V. *Phys. Rev. E* **2001**, *65*, 016 606. (e) Fistul, M. V.; Miroshnichenko, A. E.; Flach, S.; Schuster, M. Ustinov, A. V. *Phys. Rev. B* **2002**, *65*, 174 524.

(9) Kladko, K.; Malek, J.; Bishop, A. R. *J. Phys.: Condens. Matter* **1999**, *11*, L415.

(10) (a) Fehske, H.; Wellein, G.; Büttner, H.; Bishop, A. R.; Salkola, M. I. *Physica B* **2000**, *281*, *282*, 673. (b) Voulgarakis, N.; Kalosakas, G.; Bishop, A. R.; Tsironis, G. P. *Phys. Rev. B* **2001**, *64*, 020301.

(11) Clark, R. J. H.; in *Advances in Infrared and Raman Spectroscopy*; Clark, R. J. H., Hester, R. E., Eds.; Wiley Heyden: New York, 1984; Vol. 11, p 95.

(12) Keller, H. J. In *Extended Linear Chain Compounds*; Miller, J. S., Ed.; Plenum: New York, 1982; Vol. 1, p 357.

(13) Scott, B.; Love, S. P.; Kanner, G. S.; Johnson, S. R.; Wilkerson, M. P.; Berky, M.; Swanson, B. I.; Saxena, A.; Huang, X. Z.; Bishop, A. R. *J. Mol. Struct.* **1995**, *356*, 207.

(14) Huckett, S. C.; Scott, B.; Love, S. P.; Donohoe, R. J.; Burns, C. J.; Garcia, E.; Frankcom, T.; Swanson, B. I. *Inorg. Chem.* **1993**, *32*, 2137.

(15) Baeriswyl, D.; Bishop, A. R. *J. Phys. C: Solid State Phys.* **1988**, *21*, 339.

(16) Gammel, J. T.; Saxena A.; Batistic, I.; Bishop, A. R.; Phillpot, S. R. *Phys. Rev. B* **1992**, *45*, 6408.

(17) Weber-Milbrodt, S. M.; Gammel, J. T.; Bishop, A. R.; Loh, E. Y., Jr. *Phys. Rev. B* **1992**, *45*, 6435.

(18) By convention, we refer throughout to the temperature of liquid nitrogen immersed samples as 77 K and that of liquid helium immersed samples as 4 K. However, due to lowered atmospheric pressure at the 2250

m elevation of Los Alamos, the actual boiling temperature of liquid nitrogen is 75.3 K and that of liquid helium is 3.85 K. See, for example: Pobell, F. *Matter and Methods at Low Temperatures*; Springer-Verlag: New York, 1992.

(19) (a) Kubelka, P. *J. Opt. Soc. Am.* **1948**, *38*, 448. (b) Wesley, W.; Wendlandt, M.; Hecht, H. G. *Reflectance Spectroscopy*; Interscience Publishers: New York, 1966; pp 55−65.

(20) Buschmann, W. E.; et al. *Chem. Mater*. unpublished results.

(21) The *trans*-$[Pt(en)_2I_2](NO_3)_2$ starting material is synthesized by adding a 10-mL aqueous solution of $Pt(en)_2(NO_3)_2$ (0.2500 g, 0.5691 mmol) to a 10-mL MeCN solution of I_2 (0.1589 g, 0.6260 mmol) while stirring. After 5 min the red solution is diluted to 150 mL with acetonitrile and left in darkness at 10 °C. Small dark red prisms are collected after 4 days and dried under reduced pressure for 2 h to yield 0.2818 g (71%). IR (N−H): 3372 (s), 3305 (w), 3216 (sh), 3195 (w), 3120 (sh), 3034 (s), 1622 (m), 1605 (s) cm^{-1} (mineral oil). Raman (I−Pt−I): 136.7 cm^{-1} (solid); 143.0 cm^{-1} (aqueous). *Anal*. Calcd for $C_4H_8N_6O_6I_2Pt$: C, 7.01; H, 1.18; N, 12.27; I, 37.05%. Found: C, 7.08; H, 1.27; N, 12.11; I, 36.73%.

(22) Love, S. P.; Worl, L. A.; Donohoe, R. J.; Huckett, S. C.; Swanson, B. I. *Phys. Rev. B* **1992**, *46*, 813.

(23) Love, S. P.; Huckett, S. C.; Worl, L. A.; Frankcom, T. M.; Ekberg, S. A.; Swanson, B. I. *Phys. Rev. B* **1993**, *47*, 11107.

(24) Bardeau, J. F.; Bulou, A.; Swanson, B. I. *J. Raman Spectrosc.* **1995**, *26*, 1051.

(25) Kalosakas, G.; Bishop, A. R.; Shreve, A. P. *Phys. Rev. B* **2002**, *66*, 094303.

(26) (a) Huckett, S. C.; Donohoe, R. J.; Worl, L. A.; Bulou, A. D. F.; Burns, C. J.; Swanson, B. I. *Synth. Metals* **1991**, *41*, 2773. (b) Donohoe, R. J.; Worl, L. A.; Arrington, C. A.; Bulou, A. D. F.; Swanson, B. I. *Phys. Rev. B* **1992**, *45*, 13185.

(27) Bardeau, J. F.; Bulou, A.; Klooster, W. T.; Koetzle, T. F.; Johnson, S.; Scott, B.; Swanson, B. I.; Eckert, J. *Acta Cryst B* **1996**, *52*, 854.

(28) Burberry, M. S.; Albrecht, A. C. *J. Chem. Phys.* **1979**, *71*, 4631.

(29) Dexheimer, S. L.; Van Pelt, A. D.; Brozik, J. A.; Swanson, B. I. *Phys. Rev. Lett.* **2000**, *84*, 4425.

(30) Van Pelt, A. D.; Dexheimer, S. L. In *Ultrafast Phenomena XII*; Springer Series in Chemical Physics; Elsaesser, T., Mukamel, S., Murnane, M. M., Scherer, N. F., Eds.; Springer: New York, 2001**;** Vol. 66.